

Chapter 2

Basics of Ultrathin Metal Films and Their Use as Transparent Electrodes

2.1 Definition of Ultrathin Metal Films

The beginning of “Thin Film Science” can possibly be traced back to the observation of Grove [1] in 1852 who noted that metal films are formed by sputtering of cathodes with high energy positive ions. Since then it has come a long way and today it has become a fully-fledged academic discipline which has led to many industrial and household products. There is a phenomenal rise in thin metal films research, like their counterpart dielectric films, due to their extensive applications in electronics, optics, aviation, space science, defence and several other industries [2, 3]. These investigations have led to numerous inventions in the form of active devices and passive components such as piezo-electric devices, sensor elements, storage of solar energy and its conversion to other forms, reflecting and anti-reflecting coatings and many others. Furthermore, due to compactness, better performance and reliability coupled with low cost production, thin film devices and components are preferred over their bulk counterparts [4, 5].

Metal film properties are sensitive not only to their structures but also to many other parameters, including the process by which they are made, deposition conditions, substrates onto which they are deposited and most crucially on their thickness [6–8]. Basic research on thin metal films is generally limited to certain ranges of thickness, typically between a few Angstroms (\AA) to about 10,000 \AA depending on the properties under investigation. Mathematically, thin films are defined as a homogeneous solid material contained between two parallel planes and extended infinitely in two directions (x , y) but restricted along the third direction (z), which is perpendicular to the x – y plane. The dimension along the z -direction is known as the film thickness. Within the definition of thin films they can be classified according to their thickness as (i) ultrathin, (ii) thin, and (iii) comparatively thicker ones, the last one generally greater than 1000 \AA . The first category has thickness in the range of few \AA to 100 \AA while the second category falls in the regime of 100–1000 \AA . UTMFs (≤ 10 nm) find their applications in areas such as magnetic sensors, recording materials, electro-optic and novel

devices such as spin filters, transistors, solar cells, and organic LEDs. In this thesis work as mentioned in [Chap. 1](#), the UTMFs were explored and successfully used as TEs which can seriously compete with widely used indium based ITO.

2.2 Deposition of UTMFs

The existing techniques for thin film deposition are essentially based on Physical Vapor Deposition (PVD) processes: among those, the most popular ones are sputtering and thermal evaporation, but also pulsed laser ablation is gaining importance. Whichever the technique used, due to the importance of impurities and contaminants, deposition of thin films using PVD relies on ultra-high vacuum systems, i.e. base vacuum levels of $>10^{-7}$ Torr [9, 10]. Moreover, the nature of the deposited films is governed by a great variety of parameters that characterize the deposition process, such as deposition rate, pressure and composition of deposition atmosphere, cleanliness level of the vacuum chamber, substrate temperature, substrate materials, target-substrate distance, and substrate angle [8–10]. The presence of defects, dislocations, grain boundaries and surface roughness may be determinant for the film properties. In order to reach film thicknesses below 100 Å (10 nm), one must often push process parameters (such as vacuum base-level, gas pressure, power, time of exposure) to the extreme limits allowed by the deposition system themselves. This may lead to problems of film quality (for example in terms of uniformity) and repeatability. These drawbacks are critical, and have to be taken into account when dealing with industrial manufacturing.

Among the variety of PVD processes, deposition by sputtering holds a unique position. Well known advantages over evaporation processes include wide-area uniform coverage, ability to coat temperature-sensitive substrate materials, and the virtually limitless variety of materials that can be deposited [11]. Included in the latter category are metals, compounds, alloys, and mixtures. Oxide, nitride, and fluoride compounds can be reactively sputtered starting from metal targets. Many variants of sputtering exist today, with DC sputtering the most appropriate for metals while RF sputtering for dielectrics and special compositions.

The basic process of sputtering involves a process gas (in our case argon, Ar) which is introduced inside the high vacuum chamber (Fig. 2.1). An electric field is applied between the target and the substrate which leads to the creation of plasma with the positive Ar^+ ions accelerated towards the cathode (target) located on the bottom of the chamber. Particles are detached from the target due to the momentum transfer of Ar^+ ions when colliding with the target material, contained within a plasma plume similar to a flash light or a cone resulting in deposition of film on the substrate situated just above the cathode. Free electrons generated during the process are confined close to the target material using a magnetic field created by a magnet ring located just behind the cathode (target). It is then less probable that these ions recombine with free electrons in their way to the target, leading to an increased sputtering rate.

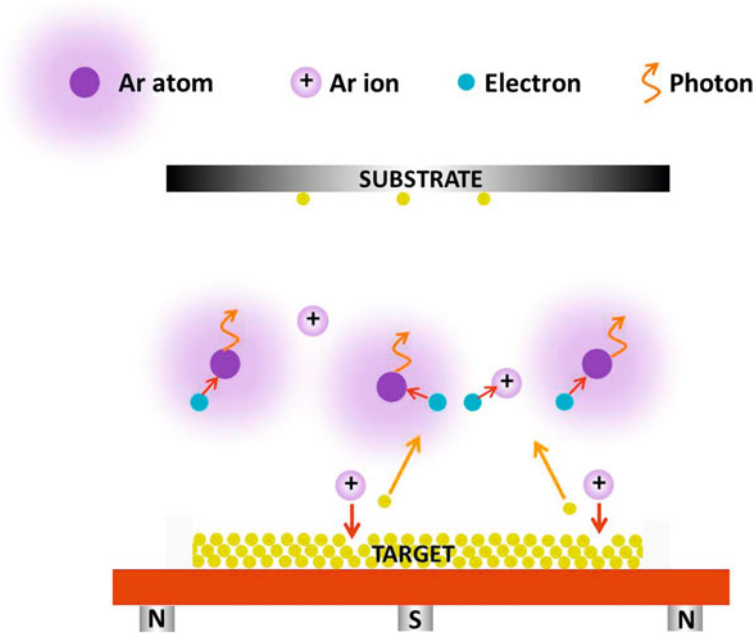


Fig. 2.1 Spatial distribution of particles inside the high vacuum sputtering chamber

In ICFO, we have two different kinds of sputtering system for deposition of UTMFs: ATC Orion 3 HV and, a more recent, advanced ATC Orion 8 HV. Both of them are magnetron sputtering systems having different configurations and are manufactured by AJA International Incorporation [12]. Orion 3 HV is a single target, low throughput R&D engine, allowing both DC and RF magnetron sputtering in pure Ar atmosphere. Its set-up is planar, with a fixed target (and magnetic field) and a pendulum oscillating platform for the substrate. No degas chamber is available and depositions can only be made at room temperature. Orion 3 HV's pumping system is composed of dry rotary vane pump which allows reaching a base vacuum pressure level of 10^{-7} Torr (4 h stand-by) in the deposition chamber. Each target has a diameter of 2 in. allowing good deposition uniformity ($<2.5\%$) over a maximum area of ~ 4 in. The ATC Orion 8 HV sputtering system instead is a computer controlled fully automatic RF/DC deposition system with co-planar configuration and can have 7 different target materials installed at the same time. The target size diameter is 2 in. and the system reaches thickness uniformity of 2.5% over 4 in. diameter substrates. It has an integrated load lock system for sample transfer without breaking the vacuum of the main chamber. The ATC Orion 8 HV has 2 radio-frequency (RF) and 2 direct current (DC) power sources which allows co-sputtering as well. The system also allows deposition at higher temperature, up to $800\text{ }^{\circ}\text{C}$ and has an O_2 reactive gas line, apart from an Ar line (process gas). Substrates are placed on a rotating sample holder that can spin

around the axis of the chamber up to a maximum rotation frequency of 40 revolutions/min. The main chamber is connected to a turbo pump which can reach a base vacuum level of 5×10^{-8} Torr in just 3 h of standby time while the load lock is pumped by a smaller rotary pump. The system is also fitted with a quartz crystal thickness monitoring unit by which the deposition rates can be deduced (Fig. 2.2).

Fig. 2.2 Picture of ATC Orion 3 HV (*top*) and ATC Orion 8 HV (*bottom*) installed at Nanophotonics lab, ICFO



Several substrates can be used for UTMF deposition according to the different experimental requirements. Electrical resistivity measurements were carried out using non-conductive substrates while transparent substrates were used for optical transmittance studies. On the contrary, experiments, such as thickness measurements, do not have any special substrate requirement and silicon substrates are thus used for this purpose while for analyzing the flexibility of the UTMFs, polyethylene terephthalate (PET) of 0.125 μm thickness were used. For device applications, such as OPVs and OLEDs, double side optically polished UV fused silica substrates were preferred. These substrates are characterized by their very low surface roughness and are transparent in the UV region of the spectrum. In order to get rid of any possible environmental contaminant a standard cleaning technique prior to the deposition has been employed for all the samples. An ultrasonic bath in acetone (10 min) followed by ethanol (10 min) was employed. The samples were then dried using a N_2 flux. The cleaned substrates were subsequently cleaned again inside the main sputtering chamber for 15 min by using either an Ar or O_2 plasma.

2.3 Growth of UTMFs

Thin film growth consists of three distinctive steps: nucleation followed by coalescence and finally thickness growth. During the early stages of thin film formation a sufficient number of vapor atoms or molecules condense and establish a permanent residence on the substrate. Many such film birth events occur in this so called nucleation stage. In the nucleation stage, a uniform distribution of small but highly mobile clusters or islands is observed. In this stage the prior nuclei incorporate impinging atoms or molecules and subcritical clusters and grow in size while the island density rapidly saturates. The next stage involves merging of the islands by a coalescence phenomenon. Coalescence decreases the island density resulting in local denuding of the substrate where further nucleation can occur. Continued coalescence results in the development of a connected network with unfilled channels in between. With further deposition, the channels fill in and shrink leaving isolated voids behind. Finally, even the voids fill in completely and the film is said to be continuous.

Generally, during the nucleation stage depending on the interaction energies of the substrate atoms and the film atoms, three growth modes are observed: (i) Frank-Van der Merwe (layer) [13], (ii) Volmer-Weber (island) [14], and (iii) Stranski-Krastanov (mixed) [15]. In 1958, Bauer gave a thermodynamic criterion for the growth mode [16]. The criteria states that under equilibrium conditions, the growth mode is determined by the following energy difference:

$$\Delta\sigma = \sigma_f + \sigma_i - \sigma_s \quad (2.1)$$

where σ_s is the surface free energy of the substrate, σ_i is the free energy of the interface, and σ_f the free energy of the film (Fig. 2.3).

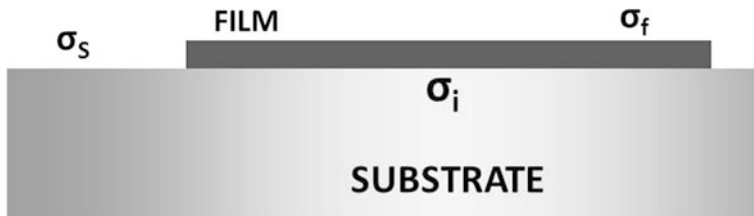


Fig. 2.3 Bauer's thermodynamic criterion for the growth mode

If $\Delta\sigma \leq 0$, the adsorbed atoms/molecules (adatoms) are more strongly bound to the substrate than to each other and the extension of the smallest stable nucleus occurs overwhelmingly in two dimensions, resulting in the formation of planar sheets. Under this condition, complete wetting of the substrate is favorable, and Frank–van der Merwe (layer-by-layer) growth should be observed. The inequality has the opposite sign when the atoms (or molecules) are more strongly bound to each other than to the substrate. In this case, one usually obtains Volmer–Weber growth (island growth), i.e., no wetting of the substrate. To predict the growth mode of UTMFs, one can look at results on metals and semiconductors deposited on oxide substrates. The film energy may have a contribution such as the strain energy, which increases linearly with increasing film thickness. After this energy is added to $\Delta\sigma$, it is possible for $\Delta\sigma$ to be smaller than zero until a certain thickness is reached and then larger than zero above this coverage. In this case, Stranski–Krastanov growth (mixed) generally occurs.

In our case, it is desired to have the percolation thickness (thickness at which the films becomes continuous) of metal films to be as low as possible. Generally, in case of metal films the adatoms are more bound to each other compared to their interaction with the substrates i.e. $\Delta\sigma \geq 0$ and therefore they grow via Volmer–Weber (island) mode. To increase the interaction energy with the substrates, as mentioned in Sect. 2.2, the substrates themselves were treated in O_2 or Ar gas plasma inside the sputtering chamber for 15 min.

2.4 Surface Analysis of UTMFs

Analyzing the surface morphology of UTMFs provides information on the structural properties of films as well as insights on electrical and optical performance. When passing from bulk to thin films, surface structures become more important in determining UTMF's properties. In particular, surface morphology dramatically affects electrical conduction. Non-conductive films might arise from sufficiently rough surfaces as a result of discontinuity. Accordingly, it is extremely important when dealing with UTMFs that the deposited films remain smooth when compared to the thickness of the layer. It is already intuitive that the surface roughness of the substrates has to be smaller than the thickness of the UTMF to be deposited if the

latter is to be continuous [17]. As mentioned earlier, we used optically polished UV fused silica substrates for UTMF deposition which are characterized by a very low surface roughness (RMS roughness: $<2 \text{ \AA}$).

We used *Veeco Digital Instrument Dimension 3100* atomic force microscope (AFM) instrument for surface roughness measurements at atomic scale. The limited scan area (usually $10 \times 10 \text{ }\mu\text{m}$) leads us to take a random area as a representative measurement for the rest of the surface. Typical 3D and profile images obtained with the AFM for Ni 5 nm and Cr 5 nm on UV fused silica substrates are shown in Fig. 2.4. Although some fluctuations larger than the thickness can be observed—suggesting that the films might have local discontinuities—the layers were found to be globally continuous as was also confirmed by electrical resistivity measurements. The raw images obtained using AFM techniques were treated using the associated software *Nanoscope Analysis*. The surface roughness is usually represented by RMS roughness (R_Q) which is given according to the following formula:

$$R_Q = \sqrt{\frac{1}{L} \int_0^L z^2(x) dx} \quad (2.2)$$

where ‘ L ’ is the evaluation length, ‘ z ’ is height and ‘ x ’ is the distance along measurement.

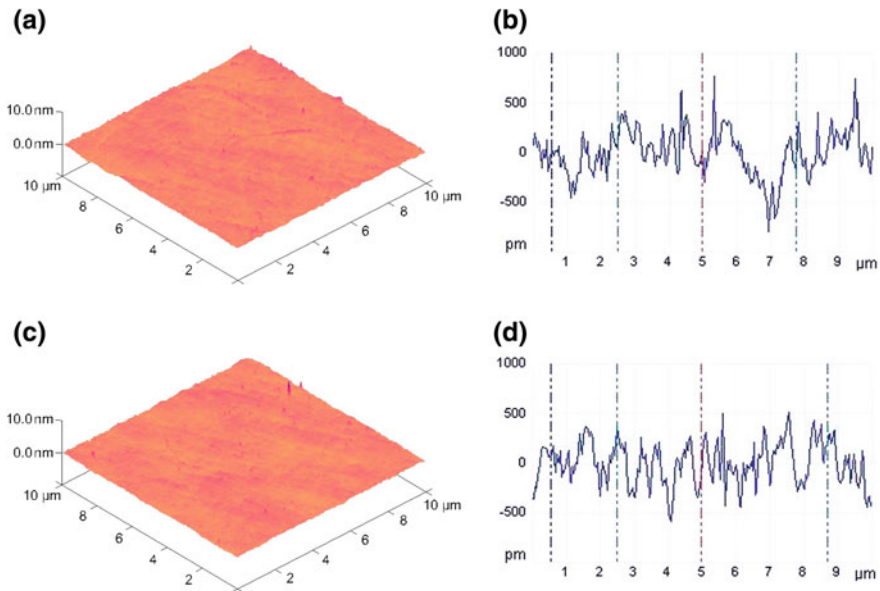


Fig. 2.4 Three dimensional and thickness profile images of Ni 5 nm (a, b) and Cr 5 nm (c, d) films on UV fused silica substrate. The RMS roughness of the films was to be 0.235 and 0.245 nm for Ni and Cr films respectively

2.5 Flexibility Analysis of UTMF

Analyzing the properties of UTMFs under stress provides information about the degree of robustness of the films. With the technology now moving toward flexible electronics with flexible OLEDs, OPV and displays, it is very important for the TEs to maintain their properties when bent. Changes in properties of TE would lead to a device with a shorter lifetime or to complete failure. To study the flexibility properties of deposited UTMFs, a set-up as shown in Fig. 2.5 was developed. The film to be analyzed is deposited onto 1×1 in. flexible substrate (generally polyethylene terephthalate (PET) or polyethylene-naphthalate (PEN) and is mounted onto the clips with two of its ends fixed. The set-up is connected to a motor which in-turn is controlled by an electronic controller which moves the arm in the horizontal direction. The cycling movement of the arm results in bending of the sample and the displacement is controlled in such a way that it makes a minimum radius of curvature of 4 mm and maximum of 12 mm on the flexible sample. The R_s value and transparency of the UTMFs is measured before and after a finite number of bending cycles to assess their flexibility and mechanical robustness.

2.6 Electrical Analysis of UTMFs

The characterization of electrical conduction of UTMFs is described in this section. By definition, intrinsic properties such as electrical resistivity or conductivity, should be constant and independent of size for a given bulk material. However, this is not true for thin films. When the film thickness becomes comparable with the characteristic length scale of a physical phenomenon, the intrinsic properties are affected by so called size-effects [18, 19]. The electrical conductivity is affected by the limitation of size as soon as film thickness becomes comparable to the electron mean free path in the medium. In the case of UTMFs, its electrical resistivity is found to be much higher than that of the corresponding bulk metal and it decreases with the increasing film thickness, eventually attaining a value often approaching that of the bulk. Before presenting the experimental results, a brief overview of the basic theory of conduction of thin metal films in the presence of enhanced size-effect is presented. The theoretical modeling of thin film resistivity is necessary for correct interpretation of experimental data.

2.6.1 Electrical Conductivity Mechanisms of UTMFs

Contrary to bulk metal, thin metallic films have one dimension, i.e. the thickness (t), which is much smaller than the other two dimensions in the plane of the film and is

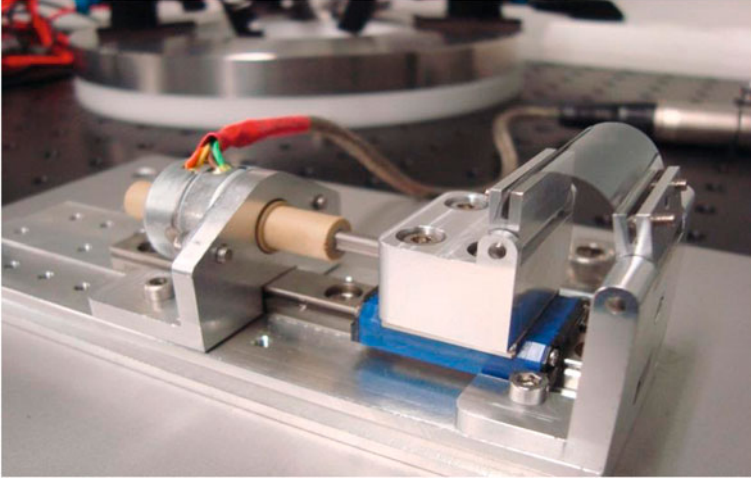


Fig. 2.5 Set-up showing the bending apparatus

comparable, in not smaller, to the electron mean free path (MFP) in bulk (l_b). In this regime, the electrical resistivity depends on the thickness of the film. Thompson considered two conditions for the calculation of thin film conductivity: (i) diffuse scattering of conduction electrons (where scattering is independent of scattering angle) by the two film surfaces, and (ii) scattering by lattice matrices where MFP of the film (l_f) will be the same as that of the bulk l_b [20]. This can be seen in Fig. 2.6.

For some arbitrary starting point ‘ z ’ within the film, electrons will be scattered in all directions. However, only in the region defined by $\Phi_2 - \Phi_1$, the electrons will be able to travel up to their MFP. While in other regions, the electrons will strike the surface of the film. From these considerations, Thomson calculated the following relations

$$l_f = \frac{3}{4}t + \frac{1}{2}t \log\left(\frac{l_b}{t}\right) \quad (2.3)$$

$$\frac{\sigma_f}{\sigma_b} = \frac{l_f}{l_b} = \frac{3t}{4l_b} + \frac{t}{2l_b} \log\left(\frac{l_b}{t}\right) \quad (2.4)$$

$$= \frac{3k}{4} + \frac{k}{2} \log \frac{1}{k} \quad (2.5)$$

where subscripts ‘ f ’ and ‘ b ’ stand for film and bulk, respectively, and $k = t/l_b$. Thompson’s approach suffers from the fact that it neglects free paths which start from the film surface.

Fuchs [21] and Sondheimer [22] (known as FS model) made a rigorous analysis of the electrical conduction process in an ideal continuous metallic film bound by two plane surfaces assuming the Boltzmann equation for the distribution function

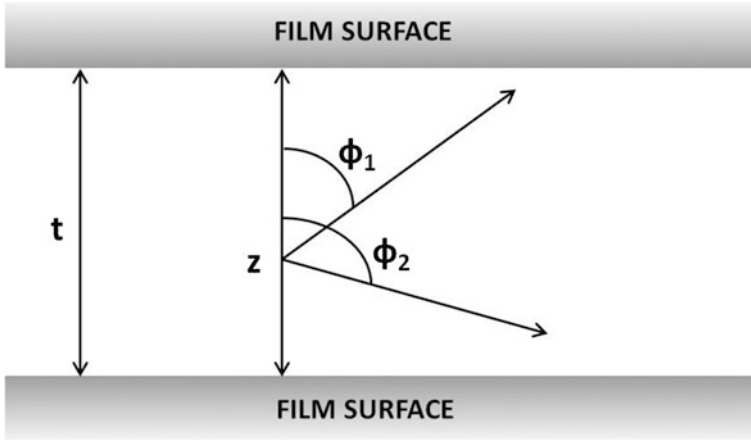


Fig. 2.6 Diffuse scattering of electrons by a film surface leading to thickness dependent mean free path l_f

and also considering the boundary scattering process. The relation between two conductivities i.e. bulk (σ_b) and film (σ_f) is then given by

$$\frac{\sigma_b}{\sigma_f} = \frac{\rho_f}{\rho_b} = \varnothing_k/k \quad (2.6)$$

where $1/\varnothing_k = (1/k) - (\frac{3}{8k^2}) + (3/2k^2) \int_1^\infty (\frac{1}{t^3} - \frac{1}{t^5}) e^{-kt} \cdot dt$.

This equation can be further simplified for thin films, i.e. $t < l_b$ or $k < 1$ to

$$\frac{\rho_f}{\rho_b} = \frac{4}{3} \frac{1}{k \{ \ln(1/k) + 0.4228 \}} \quad (2.7)$$

Sondheimer further assumed that if a fraction ' p ' of electrons is specularly scattered from the two surfaces and the rest are diffused with complete loss of their velocity, then Eq. 2.7 assumes the form

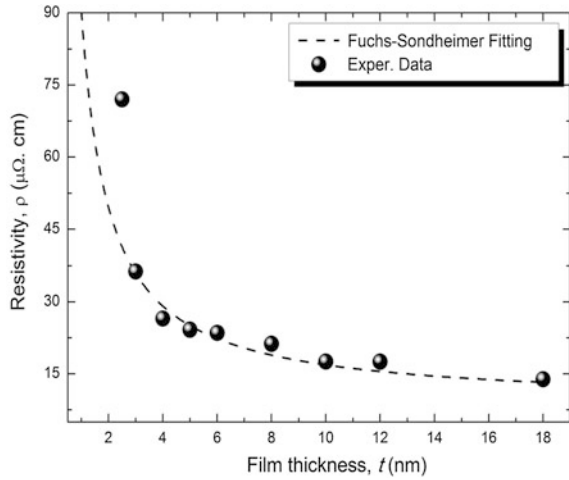
$$\frac{\rho_f}{\rho_b} = 1 + \frac{3}{8k} \quad \text{for } k \ll 1 \quad (2.8)$$

and

$$\frac{\rho_f}{\rho_b} = \frac{4}{3k} \frac{1+p}{1-p} \quad \text{for } k \gg 1 \quad (2.9)$$

Although these typical theoretical models are adequate to explain the electrical behavior of thin metal films, they might not be very accurate in the case of UTMFs. For this reason, several new approaches have been considered during the

Fig. 2.7 Experimental data for Ni layers fitted with F–S model



last decades [23, 24]. However, the FS approximation still remains the most accurate model to predict the electrical behavior of UTMFs as depicted in Fig. 2.7.

Besides geometrical limitation that enhances surface scattering, there are other sources of resistivity:

- Volume defects and impurities
- Lattice vibrations
- Strain and discontinuities, including grain boundaries.

All these are “volume” sources of scattering. Therefore, they are not included in FS expressions. As such, they should be the same for all films grown in the same conditions. Our UTMFs are polycrystalline in nature which are composed by single crystal grains. The presence of grain boundaries may reduce significantly the conductivity of metallic materials. Mayadas and Schatzkes [20] were the first to provide a model that takes into account both the scattering at external surfaces (size-effect) and scattering due to grain boundaries. They showed how a reduction of the grain size can induce a significant increase of resistivity. On the other hand, voids may also play a role in determining the electrical behavior of UTMFs. For example, an island growth can result in a discontinuous film. Even though characterized by very high resistivity, discontinuous films may still be conductive. This is due to quantum mechanical tunneling between individual islands or thermionic emission of electrons into the conduction band of the substrate [25]. UTMFs, which grow in a Volmer–Weber or island mode, present many voids between the islands which increase the resistivity by up to orders of magnitude compared to that of a uniform film (Frank–van der Merwe or layer-by-layer growth).

2.6.2 Sheet Resistance Measurement

As mentioned in the previous Sect. 2.6.1, the UTMF's electrical resistivity depends on the thickness. It is very common to measure the electrical surface properties of a film though the Sheet Resistance (R_s) in Ω/sq units:

$$\rho_t = R_s \cdot t \quad (2.10)$$

where ρ_t is the thin film electrical resistivity and t is the thickness. The sheet resistance can be measured directly using a Four-Point probe set-up connected to a multimeter. The schematic of the set-up is shown in Fig. 2.8.

To obtain the electrical resistivity of the UTMFs, the sheet resistance was measured using a *Cascade Microtech 44/7S 2791* Four Point Probe and a *Keithley 2001* multimeter. The four tips installed in the Four Point Probe were brought into contact with the layer. A test current has been injected through the outer tips while the inner tips collected the voltage drop as shown in Fig. 2.8. Typically 6 measurements were taken, each at different position on the film and the mean value of sheet resistance is calculated as:

$$R_s = C_1 \times C_2 \times R \quad (2.11)$$

where R is the average electrical resistance obtained by the multimeter and the two corrective coefficients C_1 and C_2 take into account the separation between tips (s) in the Four Point Probe Head and substrate's dimensions. In our case, the separation between tips in the four point probe head is about 1 mm and the diameter of the samples is 2.5 cm (1 in.). As UTMF thickness is always much lower than the spacing between tips, the first corrective coefficient is kept at a constant value ($C_1 = 1$) while the second one (C_2) is calculated to be 4:4364 for 1 in. substrates. We finally inferred the electrical resistivity of the layers using the definition of sheet resistance given by Eq. 2.11.

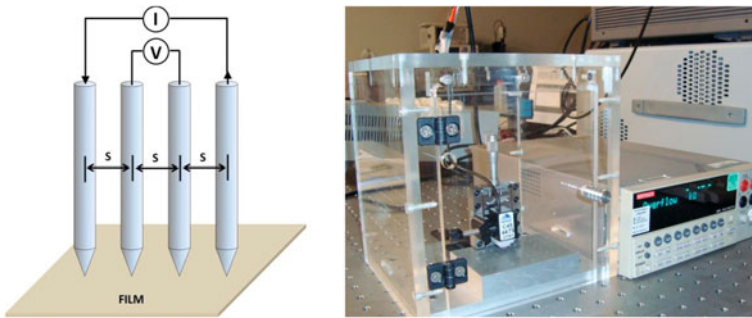


Fig. 2.8 Schematic of the Four Point probe set-up used for the sheet resistance measurement (*left*) and the actual set-up in ICFO (*right*)

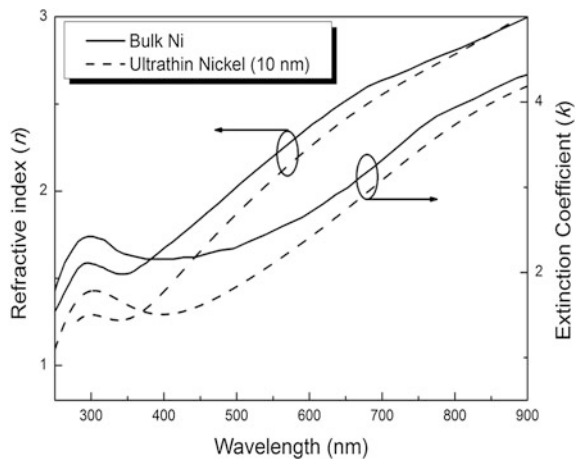
2.7 Optical Analysis of UTMFs

In order to be competitive TEs for different applications, UTMFs should keep optical losses minimum in the visible region of the spectrum. In addition, there are applications that benefit from a very broad transparency spectrum, such as ultra-violet (UV) and infra-red (IR) detectors which work with wavelengths outside the visible range. In general the response of a material to optical radiation depends on its electronic band structure. In metals the optical properties depend mainly on the contribution of the conduction band, i.e. of the free electron gas, and in some cases on intra band transitions. As long as the relaxation time of free electrons is much shorter than the period of the electromagnetic wave, the metal will exhibit a strong absorption and a high reflectivity. Indeed the extinction coefficient k of metals has very high values at low frequencies while it becomes negligible for frequencies beyond the plasma frequency, which is generally in the UV or visible region.

Thin metal films, however, present reduced optical absorption and enhanced transmission due to the reduction of thickness. Optical absorption becomes negligible when the film thickness is less than the penetration depth at optical frequencies. This is usually achievable for thicknesses <10 nm. Optical properties of UTMFs are also affected by the size-effect, since the dielectric function of metals depends mainly on the conductivity and the number of free electrons. For example, a shift of the plasma frequency should be expected when the resistivity starts to increase due to surface scatterings. Moreover, intrinsic optical properties may further differ from those of the corresponding bulk, due to the polycrystalline nature of films. Grains or macroscopic surface roughness may induce the presence of voids and discontinuities inside the volume of the metal film, giving rise to a non-uniform distribution of matter (Fig. 2.9).

As it was mentioned above, several optoelectronic devices, such as ultraviolet (UV) photodiodes, UV LEDs, solar cells for space applications, and infrared (IR)

Fig. 2.9 Comparison of optical constants of bulk and 10 nm nickel film. The measurements on UTMFs are carried out using *Sopra GES 5E Ellipsometer* while bulk values are taken from Ref. [26]. UTMFs have lower refractive index and extinction coefficient compared to their bulk counterparts

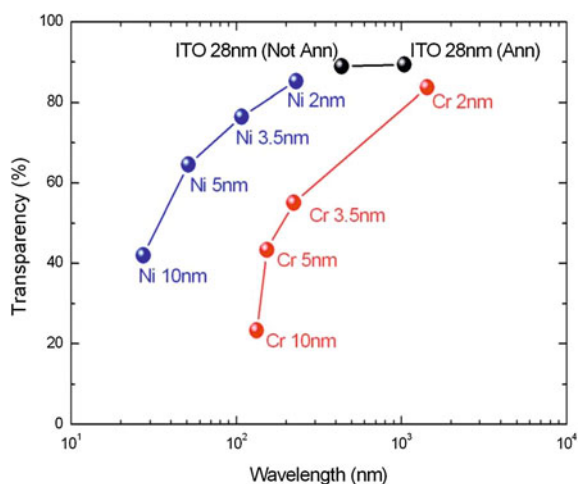


pyroelectric detectors, require electrodes with a high transparency in the UV and/or IR regions. The most widely used transparent electrodes, in particular Indium tin oxide (ITO), possess a typical band gap energy of about, $E_g = 3.75$ eV (331 nm) and plasma resonances in the near IR which makes them impractical as transparent electrodes in the UV and IR. In fact, the transparency of ITO can be increased in the near IR spectrum by reducing the free-electron density which in turn increases its resistivity [27]. Single component nickel and chromium UTMFs were deposited on UV fused silica and silicon substrates to investigate their broad spectrum optical response. Thicknesses were inferred from deposition rates determined by the quartz crystal thickness monitoring unit. They were also compared to state-of-art ITO in terms of both electrical and optical properties.

For comparison, two different ITO were grown: 28 nm as-deposited and 28 nm annealed at 450 °C for 2 h in normal atmospheric conditions. In addition, standard ITO sample (100 nm deposited onto Corning glass) was also purchased for comparison. Transmittance spectra were taken with a PerkinElmer Lambda 950 spectrometer in the UV–Visible region whereas a Shimadzu FTIR-8400S Fourier transform IR spectrometer was used in the mid-IR range. Note that substrate's contribution is always taken into account in optical transmittance measurements as $T_f = T_t/T_s$, where T_t is the total optical transmittance (film and substrate), whereas T_f and T_s are, respectively, the film and substrate optical transmittance. Electrical resistivities of the samples were measured as explained in Sect. 2.6.2.

Figure 2.10 shows the average optical transmittance in the visible range (375–700 nm) and the electrical resistivity for the Cr and Ni films of different thicknesses together with those of ITO layers, both as-deposited and annealed. In the visible range the performance of UTMFs is comparable to that of ITO. In fact, Ni films present a similar optical transparency with a significantly lower electrical resistivity. However, the real advantage of UTMFs over ITO in terms of optical transmittance is in the UV and IR ranges.

Fig. 2.10 Average optical transparency in the visible wavelengths against electrical resistivity for Cr and Ni films compared to ITO annealed and not annealed



In the UV range (175–400 nm), ITO films present enhanced absorption and therefore reduced transmittance since the material band gap is ~ 330 nm as discussed before. On the contrary, Cr and Ni films possess flatter optical transmittance with levels comparable to those in the visible range (Figs. 2.11).

Figures 2.12a and b show, respectively, the IR (from 2.5 to 25 μm) transmittance of Cr and Ni films, both being compared against ITO layers. As in the UV case, both Cr and Ni present superior optical transmittance properties: for thin samples both larger and flatter transmittance. We have also investigated the performance of standard ITO on corning glass, which presents a much faster decay of the transmission in the near IR; in fact, the transmittance goes below 20 % already at about 2.8 μm . The difference between the two ITO sets can be attributed to the

Fig. 2.11 Optical transmission of UTMFs compared to ITO annealed and as-deposited in the UV region: **a** Nickel and **b** Chromium

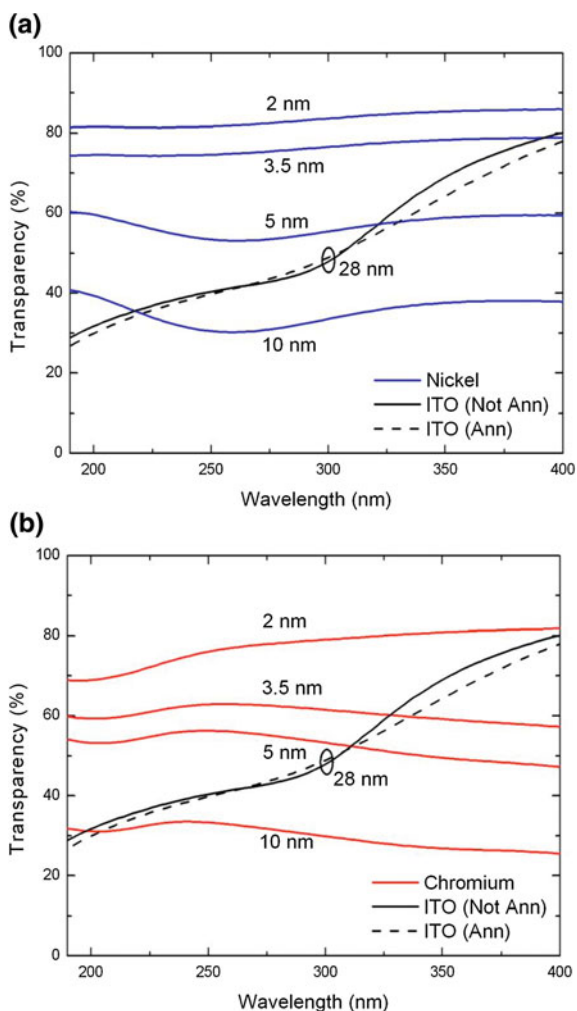
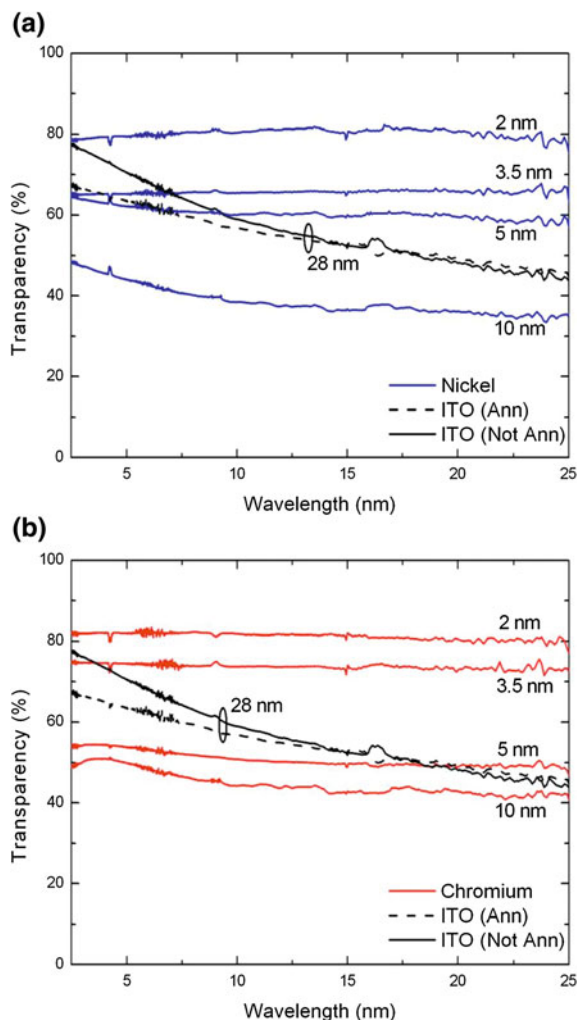


Fig. 2.12 Optical transmission of UTMFs compared to ITO annealed and not annealed in the mid-IR region: **a** Nickel and **b** Chromium



difference in free electron density [4]. The fact that the lower near-IR transparent ITO (on Corning glass) has a higher free-electron density than that of ITO on UV fused silica or Si is also confirmed by its lower electrical resistivity: about $160 \mu\Omega \times \text{cm}$ (the resistivity for ITO on UV fused silica is about $430 \mu\Omega \times \text{cm}$).

2.8 Stability

A potential drawback of UTMFs for their use as transparent electrodes is the degradation they can undergo due to oxidation when exposed to environmental agents such as air, moisture and temperature. In fact, contact with other reactive

chemical elements can also take place during fabrication (e.g. wet etching) or even be part of the structure of the device (e.g. metal/SiO₂). UTMFs are thus always at risk of changing their electrical and optical properties. This aspect is also important for non-noble metallic layers, such as chromium (Cr), nickel (Ni), titanium (Ti) and aluminum (Al).

The effect of oxidation on the electrical and optical properties of UTMFs has been investigated while, on the other hand, we take advantage to induce *ad-hoc* oxide protective layers, so that stable UTMFs can be achieved. The work was focused on Ni films, which we subjected to thermal treatment in either ambient atmosphere (~20 % of O₂) or in the presence of a continuous O₂ flow. The obtained results and techniques can be extended to other metals, such as Cr, Ti and Al.

Several Ni UTMFs of different thicknesses were grown: 2.2, 3.4, 5, and 10 nm for the stability studies. The films were kept in ambient atmosphere for 12 days to analyze the environmental effect on the films. The corresponding relative variation in electrical resistivity ($\Delta\rho/\rho$) in % was then measured for the films. It was found that, for the thinnest sample (2.2 nm) film resistivity could not be measured any longer due to its high value while 3.4, 5 and 10 nm films showed increases of 59, 16 and 4 % respectively.

The samples were then subsequently thermally treated with increasing temperature, H1 to H4 (Fig. 2.13), carried out in ambient atmosphere using a Selecta High-temp oven. The temperature was measured using a Fluke thermometer 52 II connected to an 80 PK-1 thermocouple. The electrical resistivity kept increasing after each thermal treatment for samples 3.4 and 5 nm, this effect being larger for thinner films since the formation of a natural oxide layer due to oxygen indiffusion reduces the effective metallic path, thus leading to higher electrical resistivity. A final step (H5) identical to the first one (H1) was carried out at low temperature. As it can be observed in Fig. 2.13, contrary to the initial step (H1), the electrical resistivity changes due to H5 are negligible (within 2 %) for all films, thus indicating that all UTMFs have reached high stability.

Fig. 2.13 Electrical resistivity variation after cumulative annealing treatment

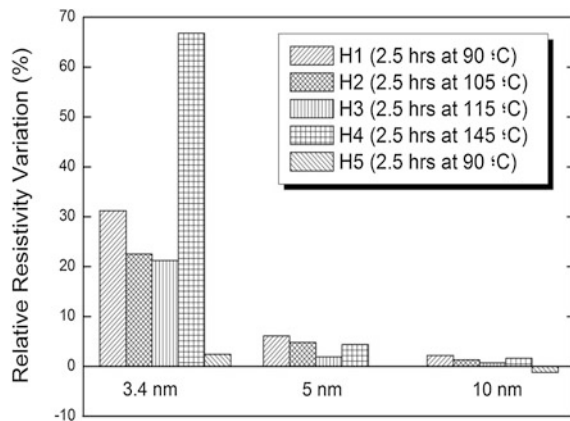
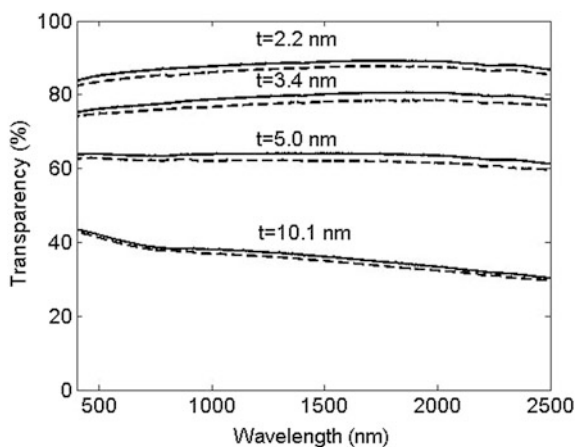


Fig. 2.14 Optical transparency of the films in the 400–2500 nm range (*dashed lines* represent as deposited samples while *solid lines* are obtained after step H5)



The optical transparency of all the samples was re-measured after the aforesaid thermal treatments and compared to that of as-deposited films (Fig. 2.14). All the samples showed increased transparency since metal oxides typically possess a lower extinction coefficient than the original metals, and the top oxide layer act as an index matching layer reducing the reflection and thus, increasing transmission [22].

In order to further elucidate the mechanism and increase the speed of the oxidation leading to stability, we subjected new Ni films to thermal treatment under a controlled dry O_2 flux. Films of different thickness were subjected to 90 min of degassing in vacuum at a temperature of about 140 °C and subsequently exposed to O_2 flux for 5 min by means of an ion gun (ion gun settings: 160 V acceleration potential and 1.8 Å ion current). The effect of oxidation can be estimated by evaluating the thickness variation of films, due to the formation of the corresponding metal oxide compound. Figure 2.15 shows the thickness scatter plot of different samples before and after the whole oxidation treatment. In case of

Fig. 2.15 Effect of oxidation on the thickness of nickel based UTMFs

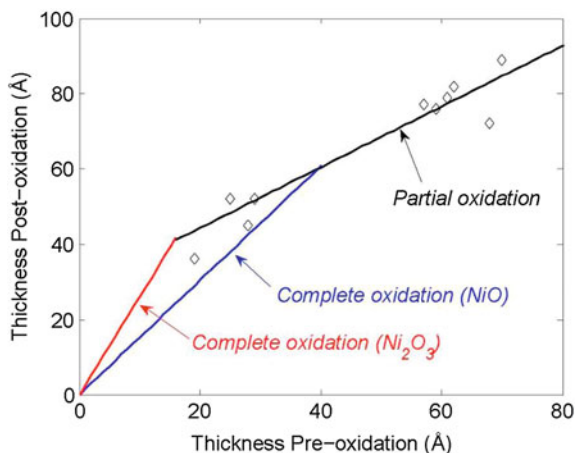


Table 2.1 Molar mass and density of nickel and its main oxide compounds Ni (II) and Ni (III)

Element	Molar mass	Density	N/N _{ox}
Nickel	58.69	8.908	
NiO	74.71	7.45	1
Ni ₂ O ₃	165.42	4.83	0.5

Last column gives the ratio between the compound number of moles over that of Ni

complete oxidation, and if the oxide compound is known, one can write the thickness ratio between metal and its oxide as:

$$\frac{t_{ox}}{t_m} = \frac{N_{ox} P_{ox} \delta_m}{N_m P_m \delta_{ox}}$$

(2.12)

where N is the number of moles, P is the molar mass and δ is the density of the material. Note that subscript m stands for metal and ox for the oxide. The main relevant parameters for Ni and its main oxide compounds are given in Table 2.1.

Given that Ni has two oxide compounds (NiO and Ni₂O₃), both corresponding complete oxidation lines are shown in Fig. 2.15 with slopes t_{ox}/t_m of 1.52 and 2.6, respectively. Completely oxidized films will increase their thickness according to a proportional factor within this interval, since the formation of a solid solution of both oxides might also be possible. However, in practice, oxidation is expected only up to a maximum thickness. Thicker layers should undergo partial oxidation for the same amount of metal thickness; in this case Eq. (2.12) will not hold. By fitting experimental data of thicker samples one obtains the partial oxidation line whose intersection point with the complete oxidation line represents the maximum oxidation thickness. According to thickness variations, the maximum oxidation thickness under the experimental conditions is in the range of 14–40 Å.

The electrical resistivity measurements of a passivated Ni 10 nm film were also carried out as a function of temperature in the 30–150 °C range (Fig. 2.16). The

Fig. 2.16 Electrical resistivity variation of passivated 10 nm nickel film with temperature

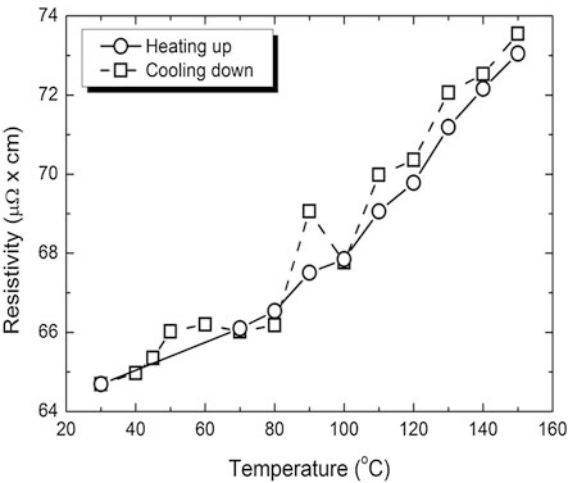


Table 2.2 Performance data of the devices with ITO and Ni electrodes

	Work function (eV)	Current density (A m^{-2})	$V_{\text{TH}}/V_{\text{maxLce}}$ (V)	Luminance (cd m^{-2})
Nickel 8 nm	5.1	5115	4.5/11	430
Nickel 10 nm	5.1	7880	4/8.5	330
ITO	5.0	7880	3.5/7.5	360

V_{TH} corresponds to the voltage at which 1 cd m^{-2} is obtained and V_{maxLce} corresponds to the voltage at which the maximum luminance is obtained

stability of the layer is confirmed by the absence of significant hysteresis, i.e., matching between “cooling-down” and “heating-up” curves. The calculated value of the temperature coefficient for the resistance (α) from Fig. 2.16 is $0.0106 \text{ }^{\circ}\text{C}^{-1}$.

2.9 Use in OLED Device

Organic LEDs were the first devices to assess the potential of UTMFs. In collaboration with Stephanie Cheylan and Danny Krautz (ICFO), single component Ni UTMF was also used, instead of ITO, as a semitransparent hole injecting electrode for bottom polymer LEDs. Standard architecture of the diodes used for the study was: Anode/PEDOT:PSS/PFO/Al, where thermally evaporated Al layer (100 nm) was used as a cathode and the active layer Poly (9,9-dioctylfluorene) (PFO) was weighed and dissolved in chloroform and stirred overnight before spin coating to make the device.

The results comparing the performance of Ni based OLEDs with that to ITO are summarized in Table 2.2.

In terms of device efficiency, a slightly higher efficiency is obtained for ITO based device at low voltages. At higher voltages, Ni based devices show a similar or improved efficiency over the ITO based device. Confinement of light modes was also calculated for both ITO and Ni based devices using a program based on the matrix transfer method. Due to the fact that the Ni was extremely thin, no confined modes are present for it, while in the case of ITO, confinement of the order of 55–65 % for both TE and TM were obtained. This explains the fact that for Ni films, despite having lower transmittance compared to ITO, the device performance is as good as that of the ITO based device.

2.10 Conclusions

We have successfully deposited UTMFs on UV fused silica and silicon substrates with high uniformity and continuity. Surface analysis of the deposited samples show that their RMS roughness is always below 1 nm. Our results show that

sufficiently thin Ni and Cr films are highly transparent in the shorter wavelengths (UV) region whereas ITO, due to its band gap, has strong absorption. In the IR region, metal layers show higher transparency while ITO has absorption due to resonance. In short, UTMFs show flatter optical transparency over the full wavelength range, from the UV to the IR (175 nm–25 μ m), still maintaining high electrical conductivity. We have also solved potential issues due to oxidation of UTMFs by intentionally growing a few nanometers top oxide layer which in turn increases stability. The resulting stabilized films present higher optical transparency while preserving adequate electrical conductivity. The measured wide optical transmission and excellent electrical properties, combined with the proven stability after an *ad hoc* passivation treatment, make UTMFs serious competitors to ITO, in particular in the UV and IR ranges. We have also investigated the possibility of using single layer Ni UTMF as an alternative semitransparent electrode for OLED applications.

We have demonstrated that similar efficiencies are reached for devices with either ITO or Ni UTMF as bottom electrode. Such results are promising, also considering that the intrinsic properties of the Ni UTMFs are not yet optimized for device applications, as it is the case for ITO.

References

1. W.R. Grove, On the electro-chemical polarity of gases. *Philos Trans R Soc Lond* **142**, 87 (1852)
2. H. Bach, D. Krause, *Thin Film on Glass* (Springer, Berlin, 1997)
3. I.B. Freund, S. Suresh, *Thin Film Materials: Stress, Defect Formation and Surface Evolution* (Cambridge University Press, New York, 2003)
4. A. Goswami, *Thin Film Fundamentals* (New Age International, New Delhi, 1996)
5. M. Ohring, *The Materials Science of Thin Films* (Academic Press, San Diego, 1992)
6. M.P. Soriaga, *Thin Films*, vol. 25 (Springer, Berlin, 2002)
7. G. Hass, Structure and optics of evaporated metals films. *Ann. Phys.* **31**, 245 (1938)
8. R. Messier, Toward quantification of thin film morphology. *J. Vac. Sci. Technol.*, A **4**, 3059 (1986)
9. J.A. Thornton, Influence of apparatus geometry and deposition conditions on the structure and topography of thick sputtered coatings. *J. Vac. Sci. Technol.* **11**, 666 (1974)
10. J.A. Thornton, Study of the microstructure of thick sputtered coatings. *Thin Solid Films* **40**, 335 (1977)
11. K. Wasa, S. Hayakawa, *Handbook of Sputter Deposition Technology: Principles, technology and Applications* (Noyes Publications, Park Ridge, 1992)
12. www.ajaint.com
13. F.C. Frank, J.H. van der Merwe, One dimensional dislocations. I. Static theory. *Proc. R. S. A* **198**, 205 (1949)
14. M. Volmer, A. Weber, Nucleus formation in supersaturated systems. *Z. Phys. Chem.* **119**, 6274 (1926)
15. J.N. Stranski, L. Krastanov, Zur Theorie der orientierten Ausscheidung von Ionenkristallen aufeinander. *Ber. Akad. Wiss. Wien* **146**, 797 (1938)
16. E. Bauer, Phenomenological theory of crystal deposition on surfaces. *Z. Kristallogr.* **110**, 372 (1958)

17. S. Giurgola, P. Vergani, V. Pruneri, Ultrathin metal films as an alternative to TCOs for optoelectronic applications. *Nuovo Cimento B* **121**, 887 (2006)
18. G. Govindaraj, V. Devenathan, Quantum size effects in thin metal films. *Phys. Rev. B* **34**, 5904 (1986)
19. Y. Choi, S. Suresh, Size effects on the mechanical properties of thin polycrystalline metals films on substrates. *Acta Mater.* **50**, 1881 (2002)
20. J.J. Thomson, *Proc. Camb Philos Soc* **11**, 119 (1901)
21. K. Fuchs, The conductivity of thin metallic films according to the electron theory of metals. *Proc. Camb. Philos. Soc.* **34**, 100 (1938)
22. E.H. Sondheimer, The mean free paths of electrons in metals. *Adv. Phys.* **1**, 1 (1952)
23. Y. Namba, Resistivity and temperature coefficient of thin metal films with rough surface. *Jpn. J. Appl. Phys.* **9**, 1326 (1970)
24. A.F. Mayadas, M. Schatzkes, Electrical resistivity model for polycrystalline films: the case of arbitrary reflection at external surfaces. *Phys. Rev. B* **1**, 1382 (1970)
25. O.S. Heavens, *Thin Film Physics* (Methuen, New York, 1973)
26. E.D. Palik, *Handbook of Optical Constants of Solids* (Academic Press, New York, 1985)
27. C.G. Granqvist, A. Hultaker, Transparent and conducting ITO films: new developments and applications. *Thin Solid Films* **411**, 1 (2002)

Ultrathin Metal Transparent Electrodes for the
Optoelectronics Industry

Ghosh, D.S.

2013, XII, 86 p. 53 illus., 34 illus. in color., Hardcover

ISBN: 978-3-319-00347-4